Ion Mobility Separation coupled with MS detects two structural states of Alzheimer's disease Aβ1-40 peptide oligomers.

Marcin Kłoniecki[1], Agnieszka Jabłonowska[1], Jarosław Poznański[1], James Langridge[3], Chris Hughes[3], Iain Campuzano[3], Kevin Giles[3] & Michał Dadlez[1, 2] *

[1]Department of Biophysics, Institute of Biochemistry and Biophysics Polish Academy of Sciences, Pawińskiego 5a, 02-106 Warsaw, Poland

[2]Institute of Genetics and Biotechnology, Faculty of Biology, University of Warsaw, Miecznikowa 1, 02-116 Warsaw, Poland

[3]Waters Corporation, Atlas Park, Simonsway, Manchester M22 5PP, UK

[1]Marcin Kłoniecki: marcinkloniecki@wp.pl;

[1]Agnieszka Jabłonowska: AJablonowska@poczta.onet.pl;

[1]Jarosław Poznański: jarek@ibb.waw.pl,

[3]James Langridge: James_Langridge@waters.com,

[3]Chris Hughes: Chris_Hughes@waters.com,

[3]Iain Campuzano: Iain_Campuzano@waters.com,

[3]Kevin Giles: kevin_Giles@waters.com,

[1, 2] *Michał Dadlez: michald@ibb.waw.pl

Corresponding author:

[1, 2] *Michał Dadlez

Department of Biophysics, IBB PAS,

Pawińskiego 5a, 02-106 Warsaw, Poland

Phone# ++48/22/592 3471

Fax# ++48/22/658 4636

e-mail: michald@ibb.waw.pl

Running Title: Aβ1-40 Oligomer Structure

Abstract

Mounting evidence points to the soluble oligomers of amyloid β peptide (Aβ) as important neurotoxic species in Alzheimer's disease, causing synaptic dysfunction and neuronal injury, and finally leading to neuronal death. The mechanism of the Aβ peptide self-assembly is still under debate. Here, Aβ1-40 peptide oligomers were studied using mass spectrometry (MS) combined with Ion Mobility Spectrometry (IMS). IMS-MS experiment allowed to separate the signals of numerous oligomers and measure their collisional cross-section values (Ω). For several oligomers at least two different species of different Ω value were detected, indicating the presence of at least two families of conformers – compact and extended. Obtained results are rationalized by a set of molecular models of Aβ1-40 oligomer structure which provided a very good correlation between the experimental and theoretical Ω values, both for the compact and extended forms. Our results indicate that MS experiment detects oligomeric species which are on-pathway in the process of fibril formation or decay, but also alternative structures which may represent off-pathway evolution of oligomers.

Keywords: Alzheimer's disease, Aβ1-40 peptide, oligomer structure, ion mobility mass spectrometry, collisional cross-section

Abbreviations used:

Aβ, amyloid β peptide; AD, Alzheimer's disease; NMR, nuclear magnetic resonance; IMS, ion mobility spectrometry; Ω, collisional cross-section; t_D, drift time; PICUP, photo-induced cross-linking of unmodified proteins; oa-ToF, orthogonal acceleration time-of-

flight; MON, monomer; DIM, dimer; TRI, trimer; TET, tetramer; PEN, pentamer; HEX, hexamer; HEP, heptamer; OCT, octamer; NON, nonamer; DEC, decamer; UDC, undecamer; DDC, dodecamer; TRD, tridecamer; TTD, tetradecamer; PND, pentadecamer; HXD, hexadecamer.

Introduction

The importance of non-monomeric species of amyloid β peptide (Aβ) in the pathogenic cascade of Alzheimer's disease (AD) is now broadly supported by a number of studies.[1-8] In the monomeric form Aβ peptide is benign, but by unknown mechanism it becomes aggregated and neurotoxic.[9] Recently mounting evidence indicates that even small, soluble oligomers can trigger synaptic dysfunction and neuronal injury.[7]

The mechanism of the Aβ peptide self-assembly is still under debate. For the last few years much effort has been directed towards characterization of the properties of Aβ oligomers.[10;11;12] The main hindrances in studies on Aβ oligomerization originate from its strong tendency to aggregate and interact with laboratory media.[13;14;15] Early *in vitro* studies conducted using the conventional techniques such as size-exclusion chromatography, ultracentrifugation, dynamic light scattering, circular dichroism, photo-induced cross-linking, electron microscopy, fluorescence resonance energy transfer or NMR brought only fragmentary information on the properties of oligomers, and no molecular structures were obtained. Recently, more detailed structural information was obtained from solid state NMR studies of oligomers stabilized into long-lived forms by specific incubation conditions. For instance forms obtained in mM concentrations of SDS,[16;17] which some authors call “artificial”,[18] or forms detected after incubation at low

temperatures[19;20] yielded a variety of model structures characterised at a different level of precision. For Aβ1-40 low temperature incubation yields relatively large β-sheet, on-pathway oligomers built of ca. 150 monomers,[19] whereas for Aβ1-42 pentameric non-β-sheet oligomers were found,[20] which were able to fibrillize upon shift to higher temperatures. SDS, on the other hand, leads to increased fibrillisation without distinct oligomeric intermediates for Aβ1-40 but for Aβ1-42 to the formation of off-pathway ordered β-sheet globular oligomers of different MW.[16;17] Obtained structures are in each case different, so no consensus pertaining the structural nature of endogenous oligomers has been reached yet. Further work is necessary to understand the mutual interdependence of these different forms and their correspondence to detected SDS-stable endogenous neurotoxic species.

The crucial limitation of the conventional techniques comes from the fact that the signals originating from structurally heterogeneous species coexisting in the solution are either averaged or heavily overlapped making them irresolvable; thus, specific information may be retrieved only for structures dominating within the population, while the presence of small fractions of potentially important species may remain undetected. To understand Aβ assembly process, during which multiple species arise, coexist and decay with time, an alternative approach is required. Mass spectrometry (MS) with its unique ability to resolve signals originating from different species co-existing in the solution, supported by the possibility to study non-covalently stabilized complexes, provides a promising alternative. The combination of Ion Mobility Spectrometry (IMS) coupled with MS expands its capabilities even further. IMS resolves species according to their collisional cross-section (Ω), providing a means to resolve isobaric species and

to measure and accurately determine their Ω. IMS-MS has recently been used to study the oligomerization of β_2-microglobulin.[21]

In our previous work[22] on Aβ truncated version spanning residues 10 through 30 (Aβ10-30) we have shown in an MS experiment, that in aqueous solution, at neutral pH, a dynamic equilibrium between Aβ10-30 monomers and a set of oligomers can be observed. Here, we extend our previous work by analyzing the oligomeric forms of a full length version of Aβ (Aβ1-40) by IMS-MS. We also construct three families of structural models which provide excellent correlation between theoretical and experimental Ω.

Results

Ion mobility separation of Aβ1-40 oligomers

In a typical MS spectrum of Aβ1-40 monomeric signals are accompanied by numerous signals corresponding to oligomers (Supplementary data Fig. S1). Some of these signals overlap, like for instance DIM^{4+} and MON^{2+}, due to equal *m/z*. Such signals can be resolved by the use of ion mobility spectrometry coupled to mass spectrometry (IMS-MS), as has previously been described.[23;24] IMS enables separation of species according to their collisional cross-section (Ω). Ions, generated in the electrospray source, entering the ion mobility device, travel towards the detector with associated drift times (t_D) linked to the Ω value by a simple formula:

(1) $$t_D^{\,X} = c*\Omega/q$$

where:

t_D – measured drift time

X – empirically estimated exponent

q – molecular charge

Ω – collisional cross-section

c – constant remaining unchanged in a single experiment.

Due to the relationship in the above equation during the course of an IMS experiment species of identical *m/z*, but with different Ω, exhibit different drift times, and can therefore be resolved. For instance two forms of lysozyme, compact and partially unfolded, were resolved using IMS.[25]

Similarly, the ToF mass spectrum of Aβ1-40 can be further resolved in an additional dimension through the use of IM coupled with oa-ToF MS (Fig. 1). The resulting dataset becomes two dimensional, with signals separated both in the domain of *m/z* and drift time and can be visualized in the form of hypsometric "heat map" with color coded signal amplitude. Again, signals expected for monomeric and non-monomeric species can be detected. Signals for monomer (MON^{2+}) and dimer (DIM^{4+}) overlapping in MS spectrum in 2164-2169 *m/z* region can be well resolved in the IMS-ToF-MS spectrum into five signal groups with different ion mobility arrival time distributions (Fig. 2). The group of signals of lowest mobility reveals a well resolved isotopic envelope of spacing 0.5 Da, corresponding to MON^{2+}. For the strongest signal the isotopic envelope allows to assign this signal to DIM^{4+}. Interestingly, two additional signals at 9.4 and 12.4 ms both represent an isotopic envelope with spacing characteristic for the +6 charge state and thus correspond to TRI^{6+}. The presence of two trimeric signals of different drift time indicates the presence of the two structurally different conformations of this oligomer, one more compact (of higher mobility) and the other one more extended. Further analysis shows that such splitting can be detected for a significant number of oligomeric forms (see below). Finally, the fifth signal corresponds to TET^{8+}. No signals of higher

oligomers (for instance PEN^{10+}, HEX^{12+} etc.) can be detected in this region of the mass spectrum, however the signals corresponding to these forms are easily detected in other regions of the mass spectrum.

Further analysis of the ion mobility separated mass spectrum (Fig. 1) at other *m/z* values reveals the presence of unique signals, which can be assigned unequivocally to the oligomeric forms, despite the partial lack of resolved isotopic envelopes. In Panel A at high *m/z* a series of unique signals can be unambiguously attributed to hexadecamer HXD^{17+} down to octamer - OCT^{9+}, forming a series of signals of oligomeric species bearing a single higher charge than the order of the oligomer (Panel A – n+1 series). At *m/z* 3789.68, two peaks were detected – at 13.4 and 14.9 ms, indicating the presence of heptamer (HEP^{8+}) and tetradecamer (TTD^{16+}). By extrapolation of the n+1 series from OCT^{9+} signal to the expected localization of HEP^{8+} signal, the signal of higher mobility (13.4 ms) at the same *m/z* value was identified as TTD^{16+} whereas the signal of lower mobility (14.9 ms) as HEP^{8+}. Following this line of reasoning all signals of n+1 series from HEX^{7+} to MON^{2+} at *m/z* 2164.62 can be identified, in agreement with the monomer (MON^{2+}) identification based on well resolved isotopic envelopes (as shown in Fig. 2). For the n+1 series signals, the drift time increases as n decreases from 10 to 3, as can be expected due to the decreasing charge present on the oligomeric species. This tendency stops at trimer TRI^{4+} and dimer DIM^{3+}, which have nearly equal arrival times (17.2 and 17.4 ms for TRI^{4+} and DIM^{3+}, respectively) and subsequently reverses for MON^{2+} (15.7 ms) which has a higher mobility than DIM^{3+}. By localizing TTD^{16+} signal assigned as described above, and unique TRD^{15+} signal the n+2 series can be extrapolated in a similar fashion through dodecamer - DDC^{14+} at *m/z* 3712.32, the

unique signal of undecamer - UDC^{13+} at *m/z* 3664.82 and further on to DEC^{12+}, NON^{11+}, OCT^{10+}, down to DIM^{4+} and MON^{3+}. The localization of DIM^{4+} and MON^{3+} by extrapolation of the n+2 series agrees well with their identification from the isotopic envelope. In spite of the significant change of charge state from +16 (tetradecamer) to +4 (dimer) the oligomeric species of n+2 series retain nearly the same drift time, between 11.0 and 13.4 ms with only a slight decrease in mobility with decreasing n. Similarly, DDC^{15+}, UDC^{14+} at *m/z* 3403.11 and DEC^{13+} at *m/z* 3331.73 start the n+3 series that can be traced to DIM^{5+} at *m/z* 1731.90. All signals expected for $MON^{2+ \div 5+}$, $DIM^{3+ \div 6+}$, $TRI^{4+ \div 7+}$, $TET^{5+ \div 8+}$, etc. up to $DEC^{11+ \div 14+}$, $UDC^{12+ \div 15+}$, $DDC^{13+ \div 15+}$, and finally HXD^{17+} forms were identified. Panel A in Fig. 1 presents the peaks corresponding to oligomeric forms, organized into three series. The formulae of the series are: $nMer^{n+1}$; $nMer^{n+2}$; $nMer^{n+3}$, where *n* is an integer corresponding to the number of units present in the species, e.g. in $nMer^{n+1}$ series, the monomer charged +2 (MON^{2+}), dimer charged +3 (DIM^{3+}), trimer charged +4 (TRI^{4+}), tetramer charged +5 (TET^{5+}), etc. were included. No charge states bearing charges higher than n+3 and lower than n+1 were identified.

Two structural conformers of Aβ1-40 oligomers

Interestingly, there still exist many strong signals that were not assigned to any of the above species. One of these signals (described in Fig. 2) represents an alternative, more extended form of the TRI^{6+} species. Similarly, other resolved mobility signals correspond to less compact conformers of other oligomers. These signals can be detected as additional strong spots at *m/z* values corresponding for instance to the identified DIM^{5+}, TET^{7+}, PEN^{8+}, HEX^{9+} signals. The identification of signals for extended

form species (denoted by "*") is shown in panel B of Fig. 1. Five series could be found n+1*, n+2*, n+3*, n+4* and an additionally split n+4** series of even lower mobility.

Extended forms are more pronounced for higher charge states of a given oligomer. This is in agreement with previous observations that more charged protein states are prone to structural destabilization in the gas phase and formation of multiple signals.[26] For instance, the comparison of the signals corresponding to PEN^{7+} with PEN^{8+} (Supplementary data Fig. S2) shows that for PEN^{7+} only the compact form is populated whereas for PEN^{8+} the signal of the extended form is stronger than the compact form. This preference for populating an extended conformer in higher charge state oligomers is also illustrated in Fig. 2, where the DIM^{4+} is present only in the compact form, whereas the TRI^{6+} is present in both forms, and the TET^{8+} only in an extended conformer. Moreover, it appears that the extended forms can accept more charge, with n+4* forms present, whereas for compact species only n+3 series are present. Higher charged species in the gas phase are known to populate more conformational states than can be detected in solution.[27] Highly charged Aβ oligomers more easily change their structure in the gas phase to extended conformations without disintegration of the oligomer by ejection of monomers.

No species bearing charge higher than n+4 were observed in the entire spectrum. This explains the lack of higher oligomeric signal (like HEX^{12+}, corresponding to n+6 series) in the *m/z* region 2164-2169. However, the signals corresponding to hexamers (and higher order oligomers) are present at higher *m/z* regions of the spectrum, bearing smaller charge and forming members of the series n+1, n+2 and n+3. In conclusion

consistent identification of the signals of oligomeric forms has been obtained in an IMS-MS spectrum.

Collisional cross-section (Ω) measurements

For each signal its associated drift time at the signal apex in the drift time domain has been measured (Table 1). Also, in the same experimental conditions the Ω values were measured for three proteins for which the Ω values are known. On this basis a calibration curve was calculated allowing for conversion of the drift time values of different Aβ1-40 oligomers, both compact and extended forms, to their Ω (Table 1), as described.[26] The Ω values of all the compact oligomeric forms but two (MON and NON) obtained for differently charged species (n+1, n+2, n+3) do not deviate by more than 5% (see column 9 of Table 1), indicating that the compact form has the same Ω value irrelevant of charge. Increasing charge density shifts the equilibrium towards the opening of the compact structure, leading to the presence of n+4*, but also an alternative n+4** forms. A slight increase in Ω value with increased charge can be observed for extended n+1* to n+4* forms (Table 1, columns 13, 15, 17, 19).

Interestingly, Ω value for the compact state increases in a linear fashion with the number of monomeric units in an oligomer (Fig. 3A), clearly indicating that even low MW oligomers attain the ordered structure, which is then propagated towards the larger forms. According to the linear regression analysis addition of each monomer leads to an increase in Ω value by an average value of 272.5±1.4 sq. angstroms. In the case of extended forms (Fig. 3B) the Ω value for lower oligomers increases by larger numbers, but for higher order oligomers (hexamer to undecamer) the increase becomes linear by an average value of 281.4±0.3 sq. angstroms, the value significantly higher than that for

the compact forms. The strong nonlinearity observed for the extended oligomers smaller than hexamer demonstrates their increasing compactness with decreasing number of monomers.

Construction of the molecular model

To rationalize the experimentally obtained Ω values we have constructed a set of molecular models of the oligomeric structure and calculated theoretical Ω values using the Waters Ω calculation algorithm (Table 1) and MOBCAL program. Results from both programs do not differ by more than 0.03%. Two alternative molecular models of the hexadecamer were constructed based on the experimental constraints known from the structure of the fibril (see Materials and Methods) and an SDS stabilized globulomer.[17]

The two experimental observations provided constraints for the selection of the molecular models. The first observation is that the IMS spectra contain well resolved peaks in the domain of the drift time, showing a narrow distribution of the Ω values for the detected oligomeric forms. This indicates that the oligomers have well defined spatial organization and thus excludes the models in which the polypeptide backbones are poorly organized. The second observation is the linear increase of Ω value with the number of monomers, clearly for compact oligomers and higher order extended oligomers (Fig. 3). The Ω value of an n-meric oligomer characterised by a fractal dimension d is expected to increase proportionally to $n^{2/d}$.[28] This means that a linear increase of Ω value (Ω ~ n) is expected for oligomers having a fractal dimension 2. This condition cannot be fulfilled in the case of monomers packing into the form of a regular sphere for which the fractal dimension is three and expected proportionality $\Omega \sim n^{2/3}$. However, the models in which monomers pack side-by-side and the oligomer grows in

two and not three dimensions have fractal dimension 2 and fulfill the above experimental constraint. In addition the selected model should be precise enough to enable atomic level molecular modeling. To our knowledge two models fulfilling the above limitations based on the experimental analysis of Aβ aggregated states exist in literature. The first is the model of a protofibril-like structure of a single β-sheet sandwich, which can be derived from a well known structure of the fibril and the second is the model of a globulomer.[17] It has to be noted however that the model of the globulomer was obtained for an oligomer of Aβ1-42 stabilized by SDS molecules, whereas in our experiment Aβ1-40 oligomers were studied in the absence of SDS.

Consequently two alternative models of the hexadecamer were constructed: a protofibril and a globulomer (Fig. 4). In panel A of Fig. 4 the protofibril model is shown with monomers aligned in a parallel two β-sheet (positions 10-22 and 29-39) sandwich with a turn at positions 23-28. In the pre-globulomer model (Fig. 4B) C-terminal parts of the monomers are engaged in an intermolecular parallel β-sheet (positions 34-40) whereas the N-terminal parts of the monomers form intramolecular hairpins spanning positions 19-22 and 30-32. In both structures side chains of negatively charged Asp23 and positively charged Lys28 form salt bridges. Interestingly, in the protofibril these interactions are intermolecular with residues from neighboring monomers engaged in the interaction and stabilizing the sandwich structure, whereas in globulomer they are intramolecular, stabilizing the hairpin turn.

The stability of the protofibril structures in high-temperature MD simulation was indeed found to be dependent on the protonation of Asp23. When, during the simulation, Asp23 side-chain were neutral the sandwich fold was easily destroyed, and oligomers adopted

the structure of two almost independent β-sheet regions (Fig. 4C). This alternative "open" structural form is a plausible candidate for the family of extended structural forms of oligomers. For 20 representative structures of protofibril and globulomer, and the last 20 snapshots of MD trajectory converging to the open form the Ω values were then calculated for each oligomer. The average values of theoretical Ω are given in Table 1, columns 10, 22, 24. The Ω values corresponding to globulomer and "open" oligomers are very similar. Also, the Ω values are calculated for truncated Aβ10-40 oligomers (Fig. 3) , as it is known that amino acids 1-9 do not participate in the stabilization of an aggregated state and are expected to be unstructured, so their impact on Ω values is difficult to model.

Correlation of theoretical and experimental Ω

Fig. 5 illustrates the correlation of the theoretical Ω calculated for the model structure of Aβ1-40 closed protofibril form (Table 1, column 10) to the measured values for the compact form (column 8) and of the theoretical open and globulomer Ω (Table 1, 22 – open, 24 – globulomer) to measured extended form (column 21). The correlation shows excellent linearity (R^2 = 0.999) even when all compact (average from n+1, n+2 and n+3 forms) and extended (n+4**) forms are taken into account. n+1*..n+4* forms have intermediate values of the Ω, most probably representing partially open structures. However, the theoretical values of the Ω are consistently larger than the corresponding measured values (Fig. 3). The larger Ω values of the model structures can be attributed to the difficulty in modeling of interactions between the N-terminal unstructured parts of individual monomers. Indeed, the Ω values of the Aβ10-40 oligomers, which are truncated by 9 residues, become significantly smaller than measured (Fig. 3, green

symbols) with the exception of the monomeric value which is still larger. It is plausible that the experimental structure of the monomer is even more compact than the most compact structure of that modeled starting from a random set of unstructured chains. It is thus also plausible that for oligomers the influence of the N-terminal unstructured region is overestimated in the Aβ1-40 model. In general however, a very good correlation between theoretical and experimental Ω values is obtained and indicates that the model rationalizes the experimental results very well. However the two models of the extended state: "open" and globulomer give similar Ω values and the Ω measurements cannot differentiate between the two models.

Discussion

Oligomers of Aβ peptide are an important element in the Alzheimer's disease puzzle, but the knowledge of their structure and assembly, which might be useful for rational drug design, is still very limited. This is due to the poor suitability of classic methods of structural analysis for the investigation of oligomers of a homogenous peptide co-existing in a dynamic equilibrium in solution, caused by averaging of the signals from different species. IMS-MS is unique in this respect in that it allows signals from different oligomeric forms to be resolved in two dimensions, namely *m/z* and Ω. In this work the application of IMS-MS provided a unique insight into the structure of Aβ oligomers and allowed us to construct a molecular model that fulfils the experimental constraints.

IMS has previously been applied to examine Aβ oligomers.[29] In that study Aβ1-42 and its P19F variant was subjected to IMS analysis, but only a few oligomeric signals were found using negative ion mode. Similarly, in a more recent study[30] only a few oligomeric signals were found in the negative ion IMS spectra of Aβ1-40. This result has been

interpreted as lack of higher oligomeric forms in the sample, contrary to the data obtained here, where the signals corresponding to a plethora of oligomeric forms were observed. A higher coverage of oligomeric signals obtained in this work almost certainly originates from the better sensitivity of positive ion ESI-MS for the Aβ oligomers and the use of more sensitive ToF detection systems. Positive ion mode spectra of [Pro^{19}]Aβ1-42 have previously been shown in Fig. S6 in ref.[30] and have been interpreted as containing only small-oligomer signals. However, in the mass spectrum shown weak signals (at ca. 1700 *m/z* and >2500 *m/z*), most probably originating from higher order oligomers, are visible, but their presence was not commented in the text. The other source of the difference in sensitivity might be a better homogeneity of the material used in our study, obtained from bacterial overexpression, compared to the chemical synthesis in the cited work. Any non-isobaric contamination at the monomer level, quite probable in the case of chemical synthesis, is expected to introduce significant non-homogeneity into the masses of oligomers and decrease the S/N value of MS signals.

In Fig. 1c and 2d in ref.[30] two profiles across z/n=-5/2 region show a split signal which was interpreted as an equilibrium between dimeric and tetrameric forms. In our dataset the signal at the corresponding region (around *m/z* 1733) is also split but the well resolved isotopic envelopes clearly indicate the presence of two dimeric forms - compact and extended (Supplementary data Fig. S3). Since in the cited work no isotopic envelope was presented we conclude that the split of this signal is shaped by the equilibrium between two structurally different dimeric forms and not the tetramer/dimer equilibrium as reported previously. The profiles at z/n=-2, (Fig. 1b in ref.[30]) corresponding to the *m/z* region 2164-2169 in our spectrum, are resolved into two

forms (monomer and dimer). This profile in our spectra is more complex, due to better resolution, both in the *m/z* and drift time domain. In addition to the monomer/dimer equilibrium observed in ref.[30], the presence of two trimeric forms and a tetrameric form are shown. Lack of signals from higher order oligomers at these two *m/z* regions of the spectra was interpreted in ref.[30] as their absence in the sample. In our work higher order oligomeric signals are also absent at these specific *m/z* regions, but they are clearly detectable in other *m/z* regions. The absence of these signals in lower *m/z* regions is not surprising as the presence of hexameric signal at *m/z* 2164.62 would require charge +12 (n+6), octameric species +16 (n+8), etc. The presence of hexameric signal at *m/z* 1731.90 would require charge +15 (n+9), octameric +20 (n+12), etc. Such highly charged forms are not observed, instead clear signals of higher order oligomeric forms with lower overall charge (not higher than n+4) are readily observed at higher *m/z* values, and a gradual decrease of charge density per monomer is observed with the oligomer order (see Supplementary data Table 1, column 5). Higher oligomeric signals are retained even after 100-fold dilution of the material (Supplementary data Fig. S4). Thus, in our opinion the IMS-MS data presented here clearly do not support the conclusion that higher order oligomeric species are not present in Aβ1-40 samples.

Equation 1 implies a linear dependence of the drift time, corrected by the exponential factor *X*, from the inversed charge.[26] Indeed the fit of equation 1 to the data for n+1, n+2 and n+3 series is very good, with the common *X* best fit value of 0.663 (Supplementary data Fig. S5). This value was previously[26] estimated to have value close to 0.5 based on the analysis of the data for large globular proteins. The value obtained here is slightly higher. This may be due to the fact that oligomers may not be spheroidal species and

thus their behavior in the ion mobility spectrometer may differ. Thus, modeling of the Aβ monomer in oligomers as quasispherical units (as applied in ref.[30]), whilst appropriate for globular proteins, may not hold for Aβ oligomers, and has no experimental support. It has been shown before for instance[22] that monomers in a dimer retain a parallel register and not the anti-parallel. Therefore a β-structure of oligomeric species is likely. We have based our molecular models on known experimental constraints and it shows good correlation with IMS data without the necessity to adjust additional parameters, like dimeric Ω value (see discussion at p. 328 in ref.[30]).

Importantly, the data obtained here shows the presence of oligomers higher than hexamers, and no indication for an abrupt decrease of oligomer population beyond hexamers could be observed. So, contrary to the conclusions of the previously cited work, the MS data presented here do not support the results of PICUP experiments[29] where a strong decrease of oligomer population beyond hexameric species was observed. Also, the dependence of the Ω values of compact oligomeric forms on charge state was not observed in our work, so it is not a general feature of Aβ oligomers, contrary to previous published conclusion (see Fig. 8 in ref.[29], Table S1, S2 in ref.[30]). In our work, a single value of Ω was obtained for compact oligomers and no assumption of the decrease of Ω value with decreasing charge was necessary to explain the obtained data. Instead, the split of the signal for oligomeric forms of higher charge was observed indicating the appearance of new structural forms with increasing charge of the molecule.

Our set of molecular models provides a probable explanation for compact/extended structural equilibrium. The basic structure detected for Aβ1-40 by MS is best modeled

by a closed protofibrillar oligomer, with the sandwich structure shielding the hydrophobic surfaces. However, also the open structures are observed most probably caused by the breakdown of the sandwich structure. The shift of the equilibrium to the open structure can be explained in the gas phase by the lack of hydrophobic interactions and in the structure of the globulomer ref.[17] by the participating SDS molecule shielding the hydrophobic patches. The opening of the protofibril may provide the bifurcation point between the on-pathway protofibril oligomers and off-pathway neurotoxic species. It can be speculated that *in vivo* some other factors, like membrane environment, can shift the equilibrium towards an open structure and lead to the formation of "off-pathway" neurotoxic species.

The two models, open and globulomer, equally well explain the collisional cross section for the extended form. However, the globulomer was shown to form in the presence of the SDS and was detected for murine Aβ1-42 containing in addition N-terminal Met residue and not for Aβ1-40.[17] The murine sequence contains three substitutions R5G, Y10F and H13R, two of them are in the part of the sequence involved in the fibril structure stabilization in Aβ1-40 and not in Aβ1-42. Therefore the globulomer was observed for a molecule which is significantly different from Aβ1-40. In addition, we observe in the gas phase that the compact-extended equilibrium is strongly influenced by charge which is most easily explained by the destabilization of the Asp23-Lys28 intermolecular salt bridge with increasing charge. Since the salt bridge exists both in closed and globulomer structure the equilibrium closed-globulomer is not expected to be charge dependent. On the contrary the equilibrium closed-open should be charge dependent since the salt bridge is absent in the open form. For these

reasons we find it most likely that the compact-extended equilibrium in the gas phase is best modeled by on-pathway protofibril-like oligomers in an equilibrium with their corresponding open forms.

We believe that this is the most comprehensive IMS-MS study to date of Aβ1-40 oligomer assembly. The use of the bacterial over-expression combined with state of the art IMS-MS methods has allowed us to produce high-quality results, clearly showing the formation of higher order oligomeric structures that may significantly expand our understanding of how soluble oligomers of Aβ form and grow either towards fibrils or to some other structures of potential neurotoxicity.

Materials and Methods

Expression and purification of Aβ1-40 peptide

The gene encoding Aβ1-40 was cloned into pET30a(+) (Novagen) plasmid, downstream of a leader sequence encoding a highly expressing variant of bovine pancreatic trypsin inhibitor.[22] For selective cleavage, the ProTEV cleavage site[31] (GluAsnLeuTyrPheGln) was inserted into the leader sequence, ahead of Aβ1-40 sequence. The transformed *E. coli* strain BL21(DE3) cells were grown from overnight cultures in LB medium supplemented with 33 μg/ml kanamycin at 37°C to A_{600} = 1.0. Protein overexpression was induced by the addition of 1 mM isopropyl-β-D-thiogalactopyranoside, followed by incubation for 2.5 hours. The cells were harvested by centrifugation and stored at –80°C. Frozen cells were thawed on ice, resuspended in 100 mM NaH_2PO_4, 10 mM Tris, 6 M GuHCl (pH 8.0), and sonicated on ice. The fusion protein was purified by Ni-NTA affinity (Qiagen) according to the manufacturer instructions, followed by purification to homogeneity on a Vydac C_{18} semi-preparative

RP-HPLC (218TP510) column and lyophilized. The purified fusion protein was resuspended in a small amount of mili-Q water acidified to pH 2.0 with hydrochloric acid and then diluted to a final concentration of 0.4 mg/ml with 50 mM Tris containing 0.5 mM EDTA and 1 mM DTT (pH 8.0). Next, 100 µl [2.25 mg/ml] of ProTEV per 4 mg of fusion protein was added in order to initiate the cleavage and the release of Aβ peptide. After 72 hours the mixture was purified by RP-HPLC using a Vydac polymer 259VHP810 column with a gradient of 23-30% solvent B over 21 min. (solvent A = 5% ACN, 10 mM NH_4OAc, pH 8.0; solvent B = 90% ACN, 10 mM NH_4OAc, pH 8.0) at 60°C. The Aβ1-40 peptide was concentrated using SpeedVac system until acetonitrile was evaporated completely. The identities of both the fusion protein and Aβ1-40 were positively verified by electrospray mass spectrometry on a Q-ToF Premier ESI-MS instrument (Waters). The concentration of the Aβ1-40 peptide stock solution, prepared as described above, was determined spectrophotometrically (Varian Cary 50 Bio) at 275 nm using molar extinction coefficient of 1410 $M^{-1}cm^{-1}$.[32] Typically the concentration of the peptide in the stock solution was within the range of 80-120 μM and, when necessary, pH was adjusted with ammonia.

Mass spectrometry experiments

Mass spectra were recorded using an ESI-Q-ToF Premier (Waters) mass spectrometer in positive ion mode either in V- or in W-mode. The instrument resolution was 10,000 for V-mode and 17,500 for W-mode (FWHM). Mass spectrometer parameters were set as follows: capillary voltage of 2.5kV, cone voltage of 35V and backing pressure of 2.00 mBar. The source and desolvation temperatures were maintained at 80 °C and 40 °C, respectively. Nitrogen was used as a cone gas with the

flow rate of 30/10 L/hour (V/W-mode respectively) and as desolvation gas with the flow rate of 650 L/hour. A standard sodium iodide solution was used for tuning and mass calibration.

Samples were infused into the mass spectrometer manually, using a glass Hamilton syringe, through a stainless steel capillary. The mass signals were measured in the range of mass-to-charge ratio (*m/z*) 500-4000 at the rate of 1 sec. per scan. The spectra analyzed were the average of 600 scans. Raw spectra were processed using MassLynx software (Waters). All data were acquired at least in triplicate to confirm the reproducibility of the results.

Ion Mobility Spectrometry – Mass Spectrometry

Experiments were performed using a Waters (Manchester, UK) Synapt G2 HDMS (high definition mass spectrometer) instrument. Synapt, described in detail elsewhere[33], has a hybrid quadrupole/ion mobility/orthogonal acceleration time-of-flight (oa-ToF) geometry. Ions are accumulated and periodically released into the mobility T-Wave cell, where they separate according to their mobility through action of a continuous train of transient voltage pulses (traveling waves) applied to the stacked ring lenses. Mobility spectra are obtained by sequentially recording two hundred ToF mass spectra following the release of the ion packet into the mobility cell. The instrument was operated in electrospray positive ion mode with a capillary voltage of 3.0 kV and sample cone 35 V. The mobility T-Wave cell was operated at a pressure of 3.2 mbar of nitrogen, with a wave velocity of 1000 m/sec and an amplitude of 40 V. Data acquisition and processing were carried out using MassLynx (V4.1) and DriftScope (V2.1) software supplied with the instrument.

The nature of the separation in the T-Wave ion mobility device is different than a drift tube since the electric field is neither constant nor uniform and, as a consequence, the relationship between the ions measured drift time (t_D) and the collisional cross section is not merely a linear relationship. However, it is possible for the T-Wave system to define and characterize the relationship between the measured drift time and collisional cross section.[34] Consequently, following the approach taken in other studies,[26;35-38] the T-Wave mobility separation has been calibrated using protein species [ubiquitin, cytochrome-C and apo-myoglobin) of known Ω values determined using standard drift tubes (http://www.indiana.edu/~clemmer/Research/cross%20section%20database/Proteins/protein_cs.htm). Previous studies have shown that calibration of the T-Wave device provides accurate Ω values in good agreement with those obtained from drift tube studies.

Modeling of Aβ1-40 oligomers

A hexadecamer of Aβ1-40 was constructed from randomly placed monomers. The structure was then optimized using simulated annealing protocol (SA) implemented in X-PLOR[39;40] with "allhdg" parameterization. For protofibril structure existing fibril structural information[41] provided constraints used in simulations: intermolecular D23-K28 salt bridge, residues L17-V24 and A30-V39 were kept in the extended conformation to build β-sheet core; the twist of the backbone in the turn region was introduced; and in agreement with mutational data, the intra-chain distance constraints (2.9-8.5 Å between C^{α} atoms) were set for F19:G38 and A21:V36 residue pairs to simulate their spatial proximity. Alternatively the topology constraints were introduced to obtain a globulomer-like structures,[17] where the residues 34-40 form an intermolecular parallel β-sheet while

residues F19-E22 and A30-I32 and intramolecular β-hairpin, separated by a short loop. The SA protocol was repeated 500 times, and for each of two variants twenty lowest energy structures were selected for further analysis. Smaller oligomers were generated from hexadecamer iteratively by the subsequent deletion of an edge monomer.

The thermodynamic stability of the two versions of the hexadecamer was tested by 1μs Molecular Dynamics run at 1000K. The final protofibril structure strictly corresponds to that of amyloid fibril reported by Petkova[41] and is denoted further as closed state, whereas the globulomer structure corresponds to the oligomer model obtained in ref.[17] Upon further simulations in the protofibril hexadecamer the three constrains stabilizing the "sandwich" structure of the closed form were purged (e.g. C^{α}-C^{α} distances in F19:G38, A21:V36 and D23:K28). D23 side-chain carboxyl group was kept either neutral or dissociated. The resulting structures are further referred to as open.

Additionally, for the Aβ1-40 monomer, 5000 SA cycles were performed in the absence of structural constrains. The conformer displaying the lowest molecular surface area was selected as model of a compact monomeric form.

For the set of the 20 lowest-energy structures representing each variant of oligomer structure (closed, open, globulomer) the theoretical Ω values were calculated using "Waters Ω" algorithm[42] and MOBCAL program.[26;43]

Acknowledgments – Many thanks to Jacek Olędzki and Agnieszka Fabijańska for help with mass spectrometry measurements, and to Nick Tomczyk and Therese McKenna for their help with the IMS-MS measurements and results. The support from Ministry of Science and Education grant N301 2543 33 is acknowledged.

References:

1. Takahashi, R. H., Almeida, C. G., Kearney, P. F., Yu, F., Lin, M. T., Milner, T. A. & Gouras, G. K. (2004). Oligomerization of Alzheimer's beta-amyloid within processes and synapses of cultured neurons and brain. *J Neurosci* **24**, 3592-9.
2. Chromy, B. A., Nowak, R. J., Lambert, M. P., Viola, K. L., Chang, L., Velasco, P. T., Jones, B. W., Fernandez, S. J., Lacor, P. N., Horowitz, P., Finch, C. E., Krafft, G. A. & Klein, W. L. (2003). Self-assembly of Abeta(1-42) into globular neurotoxins. *Biochemistry* **42**, 12749-60.
3. Kokubo, H., Kayed, R., Glabe, C. G. & Yamaguchi, H. (2005). Soluble Abeta oligomers ultrastructurally localize to cell processes and might be related to synaptic dysfunction in Alzheimer's disease brain. *Brain Res* **1031**, 222-8.
4. Barghorn, S., Nimmrich, V., Striebinger, A., Krantz, C., Keller, P., Janson, B., Bahr, M., Schmidt, M., Bitner, R. S., Harlan, J., Barlow, E., Ebert, U. & Hillen, H. (2005). Globular amyloid beta-peptide oligomer - a homogenous and stable neuropathological protein in Alzheimer's disease. *J Neurochem* **95**, 834-47.
5. Hardy, J. (2005). Expression of normal sequence pathogenic proteins for neurodegenerative disease contributes to disease risk: 'permissive templating' as a general mechanism underlying neurodegeneration. *Biochem Soc Trans* **33**, 578-81.
6. Kokubo, H., Kayed, R., Glabe, C. G., Saido, T. C., Iwata, N., Helms, J. B. & Yamaguchi, H. (2005). Oligomeric proteins ultrastructurally localize to cell processes, especially to axon terminals with higher density, but not to lipid rafts in Tg2576 mouse brain. *Brain Res* **1045**, 224-8.

7. Cappai, R. & Barnham, K. J. (2008). Delineating the mechanism of Alzheimer's disease A beta peptide neurotoxicity. *Neurochem Res* **33**, 526-32.

8. Cleary, J. P., Walsh, D. M., Hofmeister, J. J., Shankar, G. M., Kuskowski, M. A., Selkoe, D. J. & Ashe, K. H. (2005). Natural oligomers of the amyloid-beta protein specifically disrupt cognitive function. *Nat Neurosci* **8**, 79-84.

9. Lorenzo, A. & Yankner, B. A. (1994). Beta-amyloid neurotoxicity requires fibril formation and is inhibited by congo red. *Proc Natl Acad Sci U S A* **91**, 12243-7.

10. Wirths, O., Multhaup, G. & Bayer, T. A. (2004). A modified beta-amyloid hypothesis: intraneuronal accumulation of the beta-amyloid peptide--the first step of a fatal cascade. *J Neurochem* **91**, 513-20.

11. Yan, Y. & Wang, C. (2007). Abeta40 protects non-toxic Abeta42 monomer from aggregation. *J Mol Biol* **369**, 909-16.

12. Chen, Y. R. & Glabe, C. G. (2006). Distinct early folding and aggregation properties of Alzheimer amyloid-beta peptides Abeta40 and Abeta42: stable trimer or tetramer formation by Abeta42. *J Biol Chem* **281**, 24414-22.

13. Hepler, R. W., Grimm, K. M., Nahas, D. D., Breese, R., Dodson, E. C., Acton, P., Keller, P. M., Yeager, M., Wang, H., Shughrue, P., Kinney, G. & Joyce, J. G. (2006). Solution state characterization of amyloid beta-derived diffusible ligands. *Biochemistry* **45**, 15157-67.

14. Crescenzi, O., Tomaselli, S., Guerrini, R., Salvadori, S., D'Ursi, A. M., Temussi, P. A. & Picone, D. (2002). Solution structure of the Alzheimer amyloid beta-peptide (1-42) in an apolar microenvironment. Similarity with a virus fusion domain. *Eur J Biochem* **269**, 5642-8.

15. Serpell, L. C. (2000). Alzheimer's amyloid fibrils: structure and assembly. *Biochim Biophys Acta* **1502**, 16-30.

16. Rangachari, V., Moore, B. D., Reed, D. K., Sonoda, L. K., Bridges, A. W., Conboy, E., Hartigan, D. & Rosenberry, T. L. (2007). Amyloid-beta(1-42) rapidly forms protofibrils and oligomers by distinct pathways in low concentrations of sodium dodecylsulfate. *Biochemistry* **46**, 12451-62.

17. Yu, L., Edalji, R., Harlan, J. E., Holzman, T. F., Lopez, A. P., Labkovsky, B., Hillen, H., Barghorn, S., Ebert, U., Richardson, P. L., Miesbauer, L., Solomon, L., Bartley, D., Walter, K., Johnson, R. W., Hajduk, P. J. & Olejniczak, E. T. (2009). Structural characterization of a soluble amyloid beta-peptide oligomer. *Biochemistry* **48**, 1870-7.

18. Bitan, G., Fradinger, E. A., Spring, S. M. & Teplow, D. B. (2005). Neurotoxic protein oligomers--what you see is not always what you get. *Amyloid* **12**, 88-95.

19. Chimon, S., Shaibat, M. A., Jones, C. R., Calero, D. C., Aizezi, B. & Ishii, Y. (2007). Evidence of fibril-like beta-sheet structures in a neurotoxic amyloid intermediate of Alzheimer's beta-amyloid. *Nat Struct Mol Biol* **14**, 1157 - 1164.

20. Ahmed, M., Davis, J., Aucoin, D., Sato, T., Ahuja, S., Aimoto, S., Elliott, J. I., Van Nostrand, W. E. & Smith, S. O. Structural conversion of neurotoxic amyloid-beta(1-42) oligomers to fibrils. *Nat Struct Mol Biol* **17**, 561-7.

21. Smith, D. P., Radford, S. E. & Ashcroft, A. E. (2010). Elongated oligomers in ß2-microglobulin amyloid assembly revealed by ion mobility spectrometry-mass spectrometry. *Proc Natl Acad Sci U S A* **107**, 6794-8.

22. Jablonowska, A., Bakun, M., Kupniewska-Kozak, A. & Dadlez, M. (2004). Alzheimer's disease Abeta peptide fragment 10-30 forms a spectrum of metastable oligomers with marked preference for N to N and C to C monomer termini proximity. *J Mol Biol* **344**, 1037-49.

23. Giles, K., Pringle, S. D., Worthington, K. R., Little, D., Wildgoose, J. L. & Bateman, R. H. (2004). Applications of a travelling wave-based radio-frequency-only stacked ring ion guide. *Rapid Commun Mass Spectrom* **18**, 2401-14.

24. Myung, S., Lee, Y. J., Moon, M. H., Taraszka, J., Sowell, R., Koeniger, S., Hilderbrand, A. E., Valentine, S. J., Cherbas, L., Cherbas, P., Kaufmann, T. C., Miller, D. F., Mechref, Y., Novotny, M. V., Ewing, M. A., Sporleder, C. R. & Clemmer, D. E. (2003). Development of high-sensitivity ion trap ion mobility spectrometry time-of-flight techniques: a high-throughput nano-LC-IMS-TOF separation of peptides arising from a Drosophila protein extract. *Anal Chem* **75**, 5137-45.

25. Valentine, S., Anderson, J., Ellington, A. & Clemmer, D. (1997). Disulfide-Intact and -Reduced Lysozyme in the Gas Phase: Conformations and Pathways of Folding and Unfolding. *J. Phys. Chem. B* **101**, 3891-3900.

26. Ruotolo, B. T., Benesch, J. L., Sandercock, A. M., Hyung, S. J. & Robinson, C. V. (2008). Ion mobility-mass spectrometry analysis of large protein complexes. *Nat Protoc* **3**, 1139-52.

27. Wood, T. D., Chorush, R. A., Wampler, F. M., 3rd, Little, D. P., O'Connor, P. B. & McLafferty, F. W. (1995). Gas-phase folding and unfolding of cytochrome c cations. *Proc Natl Acad Sci U S A* **92**, 2451-4.

28. Tricot, C. (1981). Douze définitions de la densité logarithmique. (French) [Twelve definitions of logarithmic density]. *C. R. Acad. Sci. Paris Sér. I Math.* **293**, 549–552.

29. Bernstein, S. L., Wyttenbach, T., Baumketner, A., Shea, J. E., Bitan, G., Teplow, D. B. & Bowers, M. T. (2005). Amyloid beta-protein: monomer structure and early aggregation states of Abeta42 and its Pro19 alloform. *J Am Chem Soc* **127**, 2075-84.

30. Bernstein, S. L., Dupuis, N. F., Lazo, N. D., Wyttenbach, T., Condron, M. M., Bitan, G., Teplow, D. B., Shea, J. E., Ruotolo, B. T., Robinson, C. V. & Bowers, M. T. (2009). Amyloid-ß protein oligomerization and the importance of tetramers and dodecamers in the aetiology of Alzheimer's disease. *Nat. Chem.* **1**, 326 - 331.

31. Lucast, L. J., Batey, R. T. & Doudna, J. A. (2001). Large-scale purification of a stable form of recombinant tobacco etch virus protease. *Biotechniques* **30**, 544-554.

32. Gill, S. C. & von Hippel, P. H. (1989). Calculation of protein extinction coefficients from amino acid sequence data. *Anal Biochem* **182**, 319-26.

33. Pringle, S. D., Giles, K., Wildgoose, J. L., Williams, J. P., Slade, S. E., Thalassinos, K., Bateman, R. H., Bowers, M. T. & Scrivens, J. H. (2007). An investigation of the mobility separation of some peptide and protein ions using a new hybrid quadrupole/travelling wave IMS/oa-ToF instrument. *Int J Mass Spectrom* **261**, 1-12

34. Giles, K., Wildgoose, J. L., Langridge, D. J. & Campuzano, I. (2009). A Method for Direct Measurement of Ion Mobilities using a Travelling Wave Ion Guide. *Int J Mass Spectrom Article in Press: doi:10.1016/j.ijms.2009.10.008.*

35. Smith, D. P., Knapman, T. W., Campuzano, I., Malham, R. W., Berryman, J. T., Radford, S. E. & Ashcroft, A. E. (2009). Deciphering drift time measurements from travelling wave ion mobility spectrometry-mass spectrometry studies. *Eur J Mass Spectrom (Chichester, Eng)* **15**, 113-30.

36. Ruotolo, B. T., Hyung, S. J., Robinson, P. M., Giles, K., Bateman, R. H. & Robinson, C. V. (2007). Ion mobility-mass spectrometry reveals long-lived, unfolded intermediates in the dissociation of protein complexes. *Angew Chem Int Ed Engl* **46**, 8001-4.

37. Wildgoose, J. L., Giles, K., Pringle, S. D., Koeniger, S. L., Valentine, S. J., Bateman, R. H. & Clemmer, D. E. (2006). A Comparison of Travelling Wave and Drift Tube Ion Mobility Separations. In *Proceedings of the 54th Conference of the American Society for Mass Spectrometry, ThP05*.

38. Williams, J. & Scrivens, J. (2008). Coupling desorption electrospray ionisation and neutral desorption/extractive electrospray ionisation with a travelling-wave based ion mobility mass spectrometer for the analysis of drugs. *Rapid Commun Mass Spectrom.* **22**, 187-96.

39. Nilges, M., Kuszewski, J. & Brunger, A. T. (1991). Sampling properties of simulated annealing and distance geometry. In *Computational Aspects of the Study of Biological Macromolecules by Nuclear Magnetic Resonance Spectroscopy* (Hoch, J. C., ed.), pp. 451-455. Plenum Press, New York.

40. Nilges, M., Clore, G. M. & Gronenborn, A. M. (1988). Determination of three-dimensional structures of proteins from interproton distance data by hybrid distance geometry-dynamical simulated annealing calculations. *FEBS Lett* **229**, 317-24.

41. Petkova, A. T., Yau, W. M. & Tycko, R. (2006). Experimental constraints on quaternary structure in Alzheimer's beta-amyloid fibrils. *Biochemistry* **45**, 498-512.

42. Williams, J. P., Lough, J. A., Campuzano, I., Richardson, K. & Sadler, P. J. (2009). Use of ion mobility mass spectrometry and a collision cross-section algorithm to study an organometallic ruthenium anticancer complex and its adducts with a DNA oligonucleotide. *Rapid Commun Mass Spectrom.* **23**, 3563 - 3569.

43. Shvartsburg, A. A. & Jarrold, M. F. (1996). An exact hard-spheres scattering model for the mobilities of polyatomic ions. *Chem Phys Lett* **261**, 86-91.

Figure Legends

Fig. 1. Two-dimensional ion mobility separated mass spectrum of 200 μM Aβ1-40 in 10 mM ammonium acetate, pH 7.4. *m/z* values are shown at vertical axis and ion mobility drift time at horizontal axis. The signal amplitude is color coded increasing from purple (low intensity) to bright yellow (high intensity). The peak apexes have been accentuated by dot and the corresponding Aβ1-40 oligomeric species identity tag. For clarity the tag has been shortened to 2^{4+}, denoting +4 charged dimer, 3^{5+} denoting +5 charged trimer, etc. Panels A & B represent the results of the same experiment, with identity tags divided for clarity between compact forms oligomeric signals (A) and extended forms oligomeric signals (B). Peak identity tags were assigned as described in the text.

Fig. 2. Enlarged fragment of IMS-MS spectrum from Fig. 1. Panel A shows the range of 2164-2169 *m/z*. The colored spots indicate MS peaks with amplitude increasing from purple to yellow. At the drift time of 15.7 ms, the lowest mobility group of signals reveals a well resolved isotopic envelope of spacing 0.5 Da, indicating a charge of +2 and an associated molecular monoisotopic mass of 4327.15 Da, corresponding to a monomer MON^{2+}. For the strongest signal, of intermediate drift time (11.1 ms), the isotopic envelope allows calculation of the charge state as +4 and an associated molecular mass of 8654.3 Da, as expected for the dimer DIM^{4+}. Two additional signals at 9.4 and 12.4 ms both represent an isotopic envelope with spacing characteristic for the +6 charge state and thus correspond to the mass of a trimeric TRI^{6+} species. Also a weak signal of a tetramer charged +8 (TET^{8+}) was detected in this region. Panel B shows a projection of this spectrum region on the drift time axis (vertical axis – signal intensity). It shows relative amplitudes of the five signal groups.

Fig. 3. The dependence of the measured (red symbols) and theoretical (black or blue symbols) collisional cross-section (Ω) on the number of Aβ1-40 monomers in the oligomer. Panel A corresponds to compact form and panel B to extended form. Also, the theoretical Ω values for the truncated peptide Aβ10-40 are shown (green symbols). Linear regression best fit lines to Ω experimental values for higher order (larger than hexamer) extended oligomers is shown. The linear dependence of Ω from the number of monomers indicates a fractal dimension 2 for their structures. For lower order extended oligomer a strong deviation from linearity can be observed indicating an increase of fractal dimension of their structure and their increasing compactness.

Fig. 4. Model of closed (panel A) globulomer (panel B) and open (panel C) form of Aβ1-40 peptide hexadecamer.

Fig. 5. Correlation between measured values of collisional cross-section of Aβ1-40 oligomers (horizontal axis) and the theoretical values calculated from the molecular model (vertical axis). A good linear fit is obtained both for compact forms (R^2=0.9995 – black, filled diamond) with closed model and extended forms either with open forms (R^2=0.9989 – red, open diamond) or globulomer forms (R^2=9983, blue, open triangle). Experimental values for the compact form are the average values obtained for n+1, n+2 and n+3 series (Table 1). Extended forms are represented by the values of n+4** form. In general the model explains well the relative Ω values obtained for both forms in the experiment. In absolute terms the theoretical model gives Ω values larger than experimental by 509 $Å^2$ for the compact form, and for the extended form by 283 $Å^2$ (open) and 175 $Å^2$ (globulomer), as shown by extrapolation of the linear fit to 0.

Table 1. Experimental values[a] of IMS drift times (t_D) and collisional cross-section (Ω) and theoretical values[b] of Ω calculated based on the molecular model[c]

1	2	3	4	5	6	7	8	9	10	11	12	13	14	15	16	17	18	19	20	21	22	23	24	25
No. of mo-no-mers	**Experimental (Compact)**								**Theoretical**		**Experimental (Extended)**										**Theoretical**			
	n+1		n+2		n+3		Av.		**Closed**		n+1*		n+2*		n+3*		n+4*		n+4**		**Open**		**Globulomer**	
	t_D	Ω	t_D	Ω	t_D	Ω	Ω	Std. dev.	Ω	Error	t_D	Ω	t_D	Ω	t_D	Ω	t_D	Ω	t_D	Ω	Ω	Error	Ω	Error
1	*15.7*	600	*8.6*	597	*6.4*	647	**615**	28	**1011**	29					*7.0*	689	*5.9*	770	*6.3*	**805**	**1171**	31	**1017**	39
2	*17.4*	966	*11.1*	944	*8.1*	952	**954**	11	**1382**	33					*10.6*	1149			*9.9*	**1313**	**1668**	31	**1631**	91
3	*17.2*	1278	*12.0*	1247	*9.4*	1269	**1265**	16	**1693**	33			*15.4*	1481	*12.4*	1533	*10.6*	1606	*12.0*	**1747**	**2089**	42	**2145**	72
4	*16.6*	1562	*12.4*	1532	*10.0*	1546	**1547**	15	**1988**	33			*15.6*	1791	*13.2*	1867			*13.6*	**2179**	**2461**	48	**2585**	85
5	*16.1*	1828	*12.6*	1802	*10.4*	1810	**1813**	13	**2239**	28			*16.2*	2147	*13.6*	2175	*12.1*	2256	*14.2*	**2520**	**2848**	36	**3038**	137
6	*15.5*	2078	*12.6*	2062	*10.8*	2094	**2078**	16	**2515**	19			*16.0*	2433	*13.9*	2482			*14.6*	**2850**	**3199**	40	**3443**	119
7	*14.9*	2318	*12.6*	2317	*11.5*	2429	**2355**	64	**2756**	34			*15.9*	2723	*14.1*	2783	*12.8*	2865	*14.7*	**3159**	**3551**	34	**3686**	109
8	*14.5*	2558	*12.7*	2592	*11.8*	2716	**2622**	83	**3030**	24	*18.2*	2988	*15.8*	3015	*14.2*	3077			*14.8*	**3456**	**3883**	52	**4069**	132
9	*14.2*	2807	*12.9*	2885	*12.1*	3006	**2899**	100	**3269**	28	*17.7*	3258	*15.7*	3303	*14.2*	3365	*13.2*	3463	*14.8*	**3738**	**4237**	56	**4314**	114
10	*14.1*	3069	*13.2*	3191	*11.8*	3199	**3153**	73	**3533**	27	*17.2*	3514			*14.2*	3646			*14.7*	**4020**	**4554**	58	**4695**	90
11	*14.3*	3378	*12.9*	3412	*11.7*	3424	**3405**	24	**3777**	44	*16.9*	3790	*15.6*	3885	*14.1*	3907	*13.1*	3976	*14.7*	**4300**	**4901**	48	**4883**	173
12	*14.3*	3656	*13.4*	3766	*11.6*	3660	**3694**	62	**4035**	47	*16.5*	4032	*15.1*	4091	*14.1*	4176					**5242**	71	**5242**	136
13	*14.4*	3953	*13.4*	4039			**3996**	61	**4281**	38			*15.0*	4364							**5602**	59	**5666**	176
14	*14.4*	4247	*13.4*	4308			**4278**	43	**4557**	48											**5937**	68	**5941**	153
15	*14.4*	4515					**4515**		**4820**	50											**6286**	69	**6262**	144
16	*14.5*	4832					**4832**		**5090**	48											**6654**	85	**6502**	130

[a] (columns 2 - 9 and 12 - 21);

[b] (columns 10 - 11 and 22 - 25);

[c] Results for the compact n+1 to n+3 species (columns 2 - 7) are shown along with the averaged value of the compact species Ω (column 8) with the standard deviation (column 9). For extended species (denoted by "*") experimental results are obtained for n+1* to n+4* and n+4** series (columns 12 - 21). Theoretical Ω values were calculated for the three models of oligomers named closed (column 10), open (column 22) and globulomer (column 24) of full length peptide Aβ1-40. Errors of Ω calculation are also shown (columns 11, 23, 25).

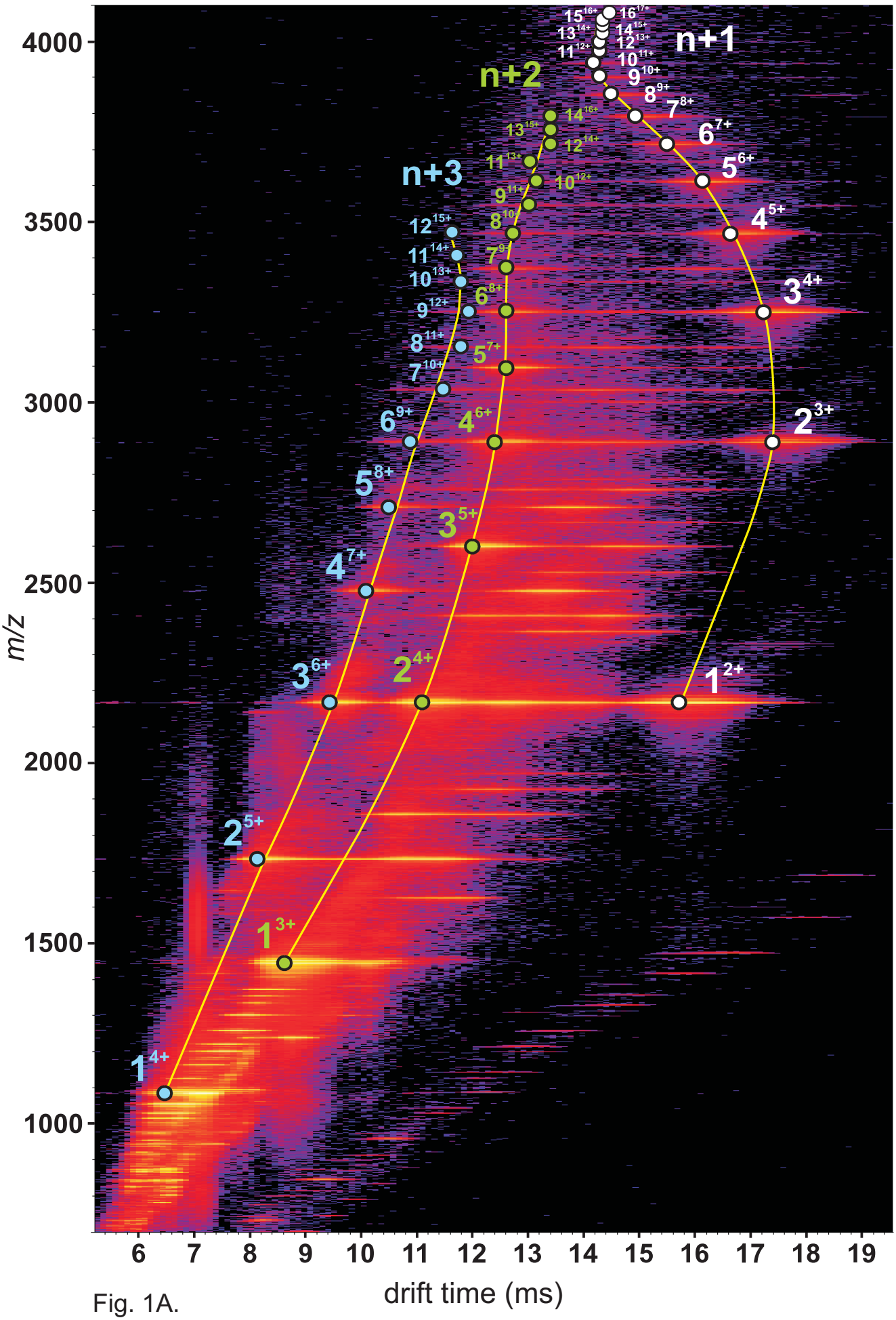
n+1
n+2
n+3
m/z
drift time (ms)
4000
3500
3000
2500
2000
1500
1000
6
7
8
9
10
11
12
13
14
15
16
17
18
19

Fig. 1A.

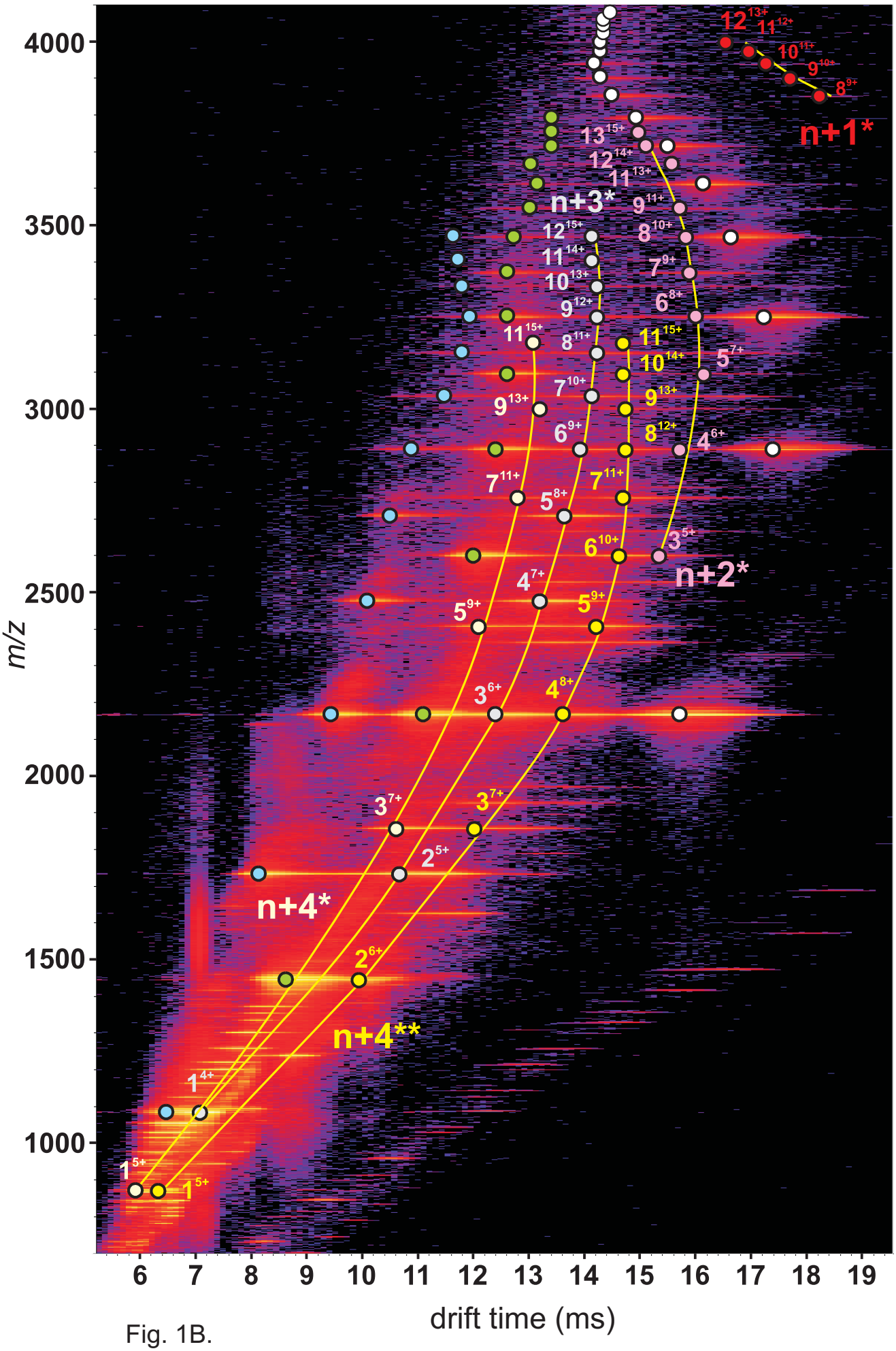

Fig. 1B.

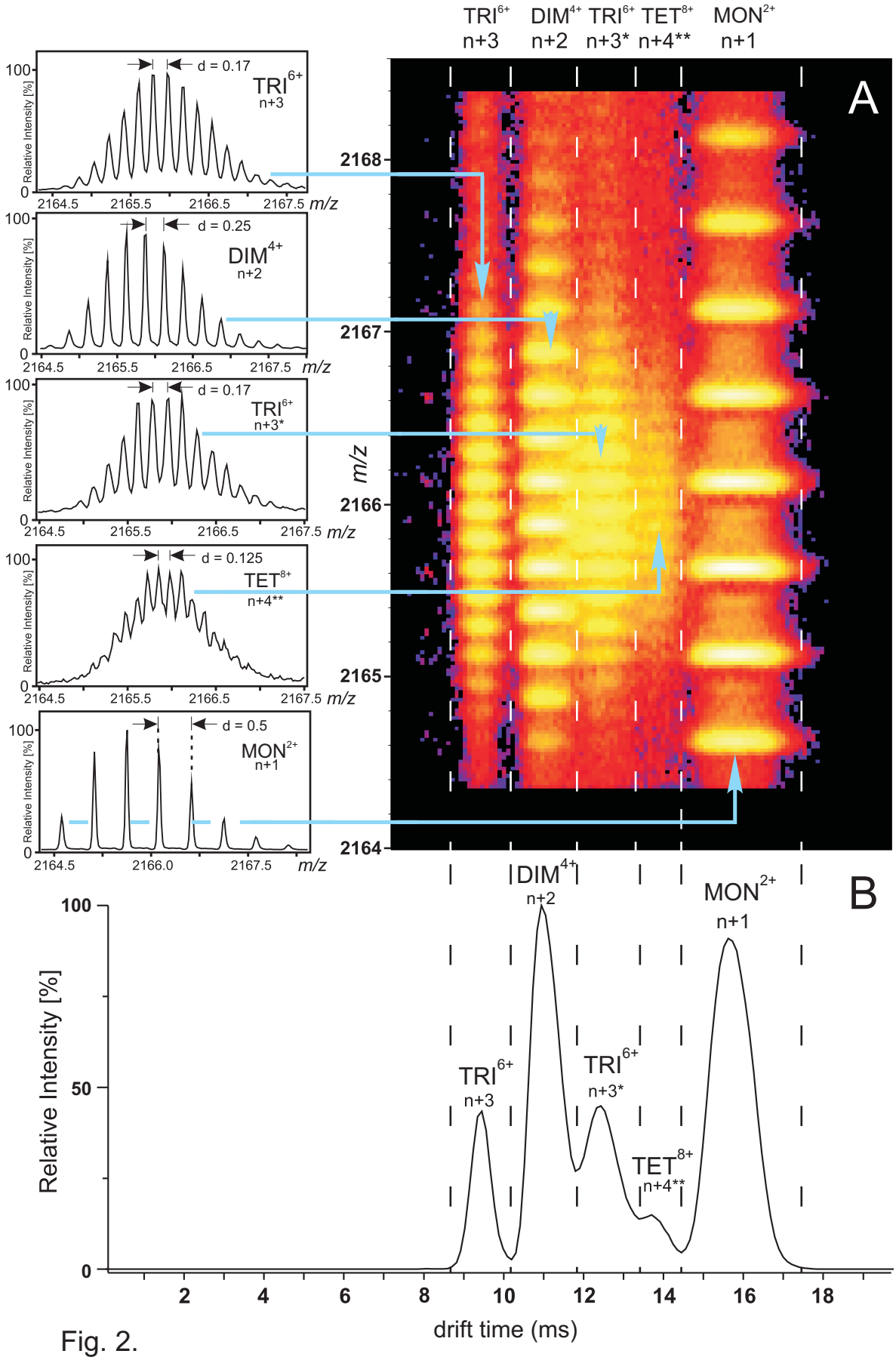
TRI6+ n+3
DIM4+ n+2
TRI6+ n+3*
TET8+ n+4**
MON2+ n+1
A
B
d = 0.17
d = 0.25
d = 0.17
d = 0.125
d = 0.5
Relative Intensity [%]
m/z
drift time (ms)

Fig. 2.

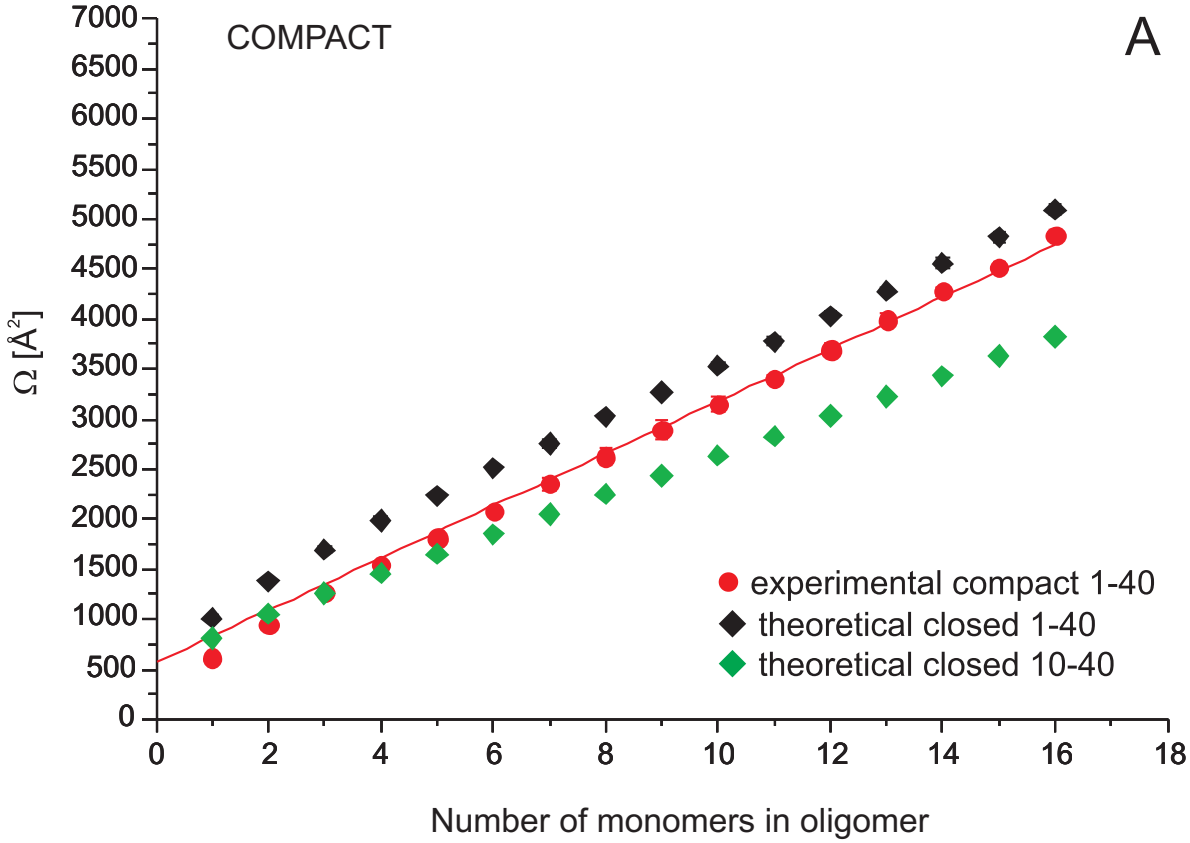
COMPACT
A
Ω [Å²]
experimental compact 1-40
theoretical closed 1-40
theoretical closed 10-40
Number of monomers in oligomer

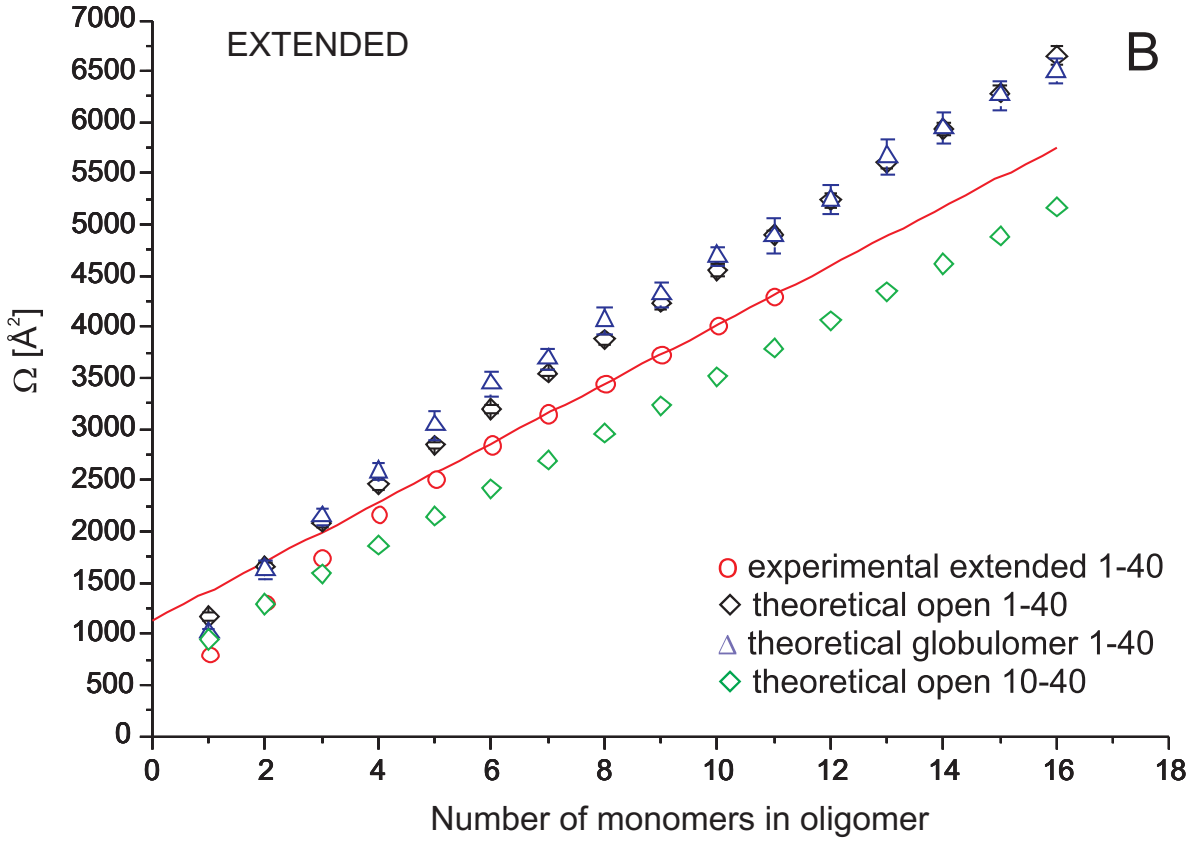
EXTENDED
B
Ω [Å²]
experimental extended 1-40
theoretical open 1-40
theoretical globulomer 1-40
theoretical open 10-40
Number of monomers in oligomer

Fig. 3.

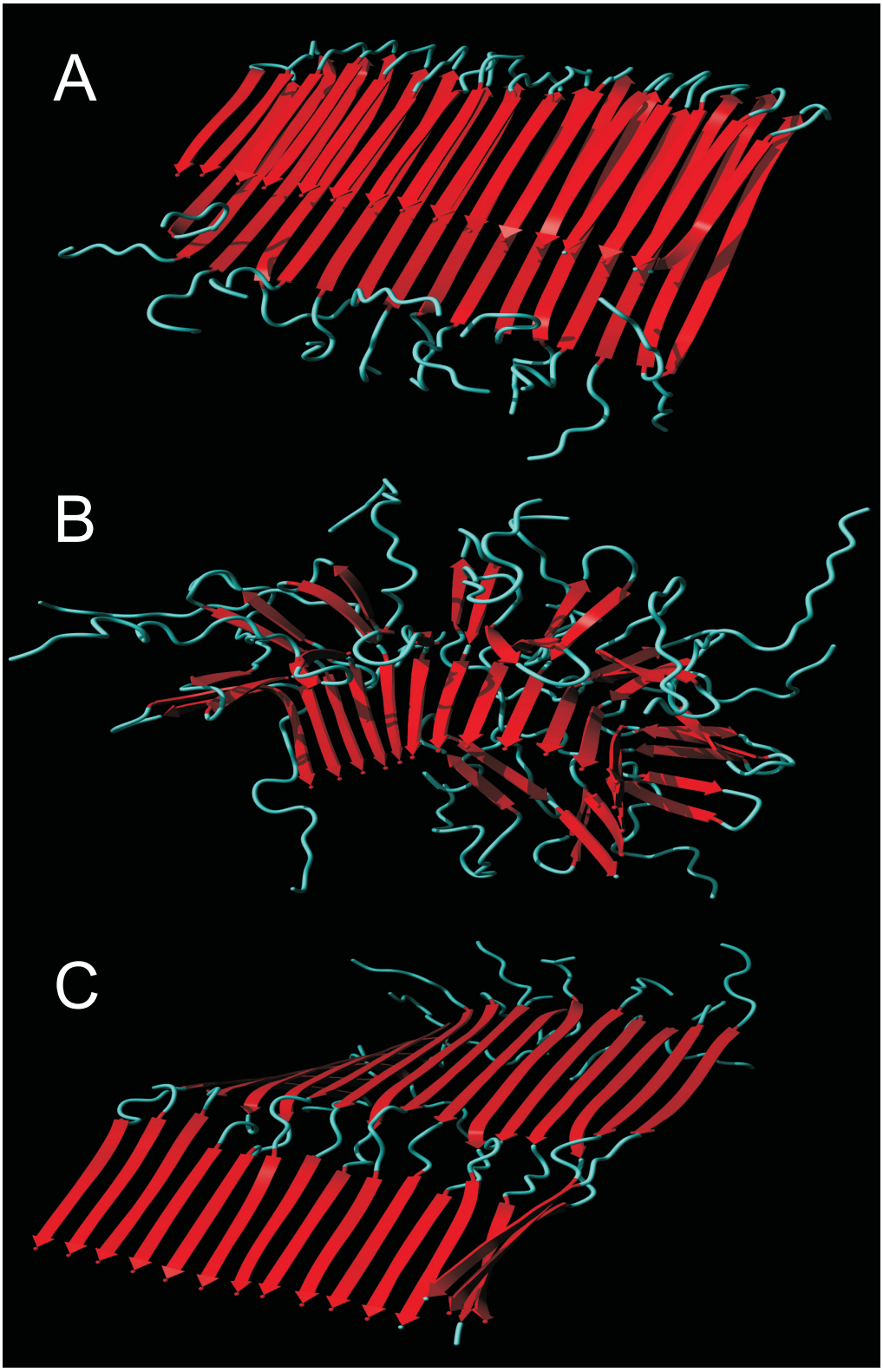

Fig. 4.

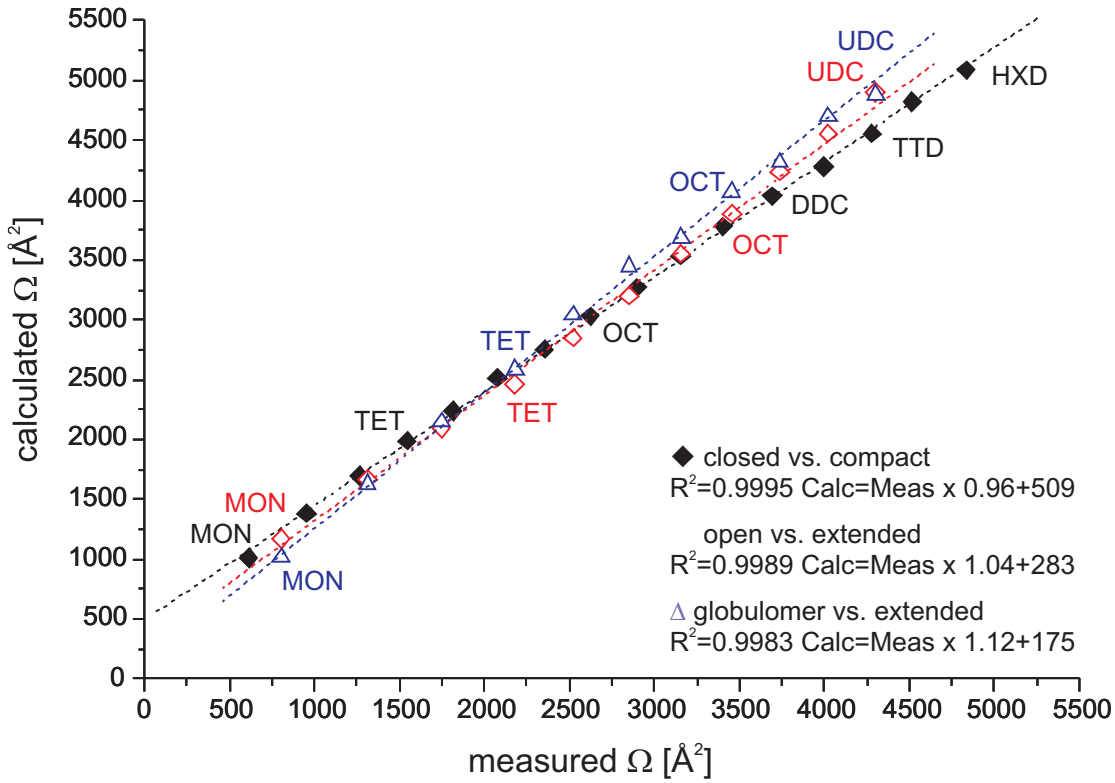
calculated Ω [Å²]
measured Ω [Å²]
0
500
1000
1500
2000
2500
3000
3500
4000
4500
5000
5500
UDC
UDC
HXD
TTD
OCT
DDC
OCT
OCT
TET
TET
TET
MON
MON
MON
closed vs. compact
R²=0.9995 Calc=Meas x 0.96+509
open vs. extended
R²=0.9989 Calc=Meas x 1.04+283
globulomer vs. extended
R²=0.9983 Calc=Meas x 1.12+175

Fig. 5.